

# UC San Diego

## UC San Diego Previously Published Works

### Title

Shake-table test performance of an inertial force-limiting floor anchorage system

### Permalink

<https://escholarship.org/uc/item/33j5w706>

### Journal

Earthquake Engineering & Structural Dynamics, 47(10)

### ISSN

0098-8847

### Authors

Zhang, Zhi  
Fleischman, Robert B  
Restrepo, Jose I  
et al.

### Publication Date



2018-08-01

### DOI

10.1002/eqe.3047

Peer reviewed

# Shake-table test performance of an inertial force-limiting floor anchorage system

Zhi Zhang<sup>1</sup>  | Robert B. Fleischman<sup>2</sup> | Jose I. Restrepo<sup>3</sup> | Gabriele Guerrini<sup>4</sup> | Arpit Nema<sup>3</sup> | Dichuan Zhang<sup>5</sup> | Ulina Shakya<sup>6</sup> | Georgios Tsampras<sup>7</sup>  | Richard Sause<sup>8</sup>

<sup>1</sup>Thornton Tomasetti, New York, NY, USA

<sup>2</sup>Department of Civil Engineering and Engineering Mechanics, University of Arizona, Tucson, AZ, USA

<sup>3</sup>Department of Structural Engineering, UCSD, La Jolla, CA, USA

<sup>4</sup>Department of Civil Engineering and Architecture, University of Pavia, Pavia, Italy

<sup>5</sup>Nazarbayev University, Astana, Republic of Kazakhstan

<sup>6</sup>CEEM Department, University of Arizona, Tucson, AZ, USA

<sup>7</sup>Simpson Gumpertz & Heger Inc., Waltham, MA, USA

<sup>8</sup>ATLSS Engineering Research Center, Department of Civil and Environmental Engineering, Lehigh University, Bethlehem, PA, USA

## Correspondence

Fleischman R, Department of Civil Engineering and Engineering Mechanics, University of Arizona, Tucson, AZ 85721-0072, USA.

Email: rfleisch@email.arizona.edu

## Funding information

National Science Foundation (NSF), Division of Civil, Mechanical and Manufacturing Innovation, Grant/Award Number: CMMI-1135033; Fund of Social Development at the Nazarbayev University, Grant/Award Number: N0KΦ-14/03; Prestressed/Precast Concrete Institute (PCI); Charles Pankow Foundation; PCI West; Clark Pacific

## Summary

A new floor connecting system developed for low-damage seismic-resistant building structures is described herein. The system, termed Inertial Force-Limiting Floor Anchorage System (IFAS), is intended to limit the lateral forces in buildings during an earthquake. This objective is accomplished by providing limited-strength deformable connections between the floor system and the primary elements of the lateral force-resisting system. The connections transform the seismic demands from inertial forces into relative displacements between the floors and lateral force-resisting system. This paper presents the IFAS performance in a shake-table testing program that provides a direct comparison with an equivalent conventional rigidly anchored-floor structure. The test structure is a half-scale, 4-story reinforced concrete flat-plate shear wall structure. Precast hybrid rocking walls and special precast columns were used for test repeatability in a 22-input strong ground-motion sequence. The structure was purposely designed with an eccentric wall layout to examine the performance of the system in coupled translational-torsional response. The test results indicated a seismic demand reduction in the lateral force-resisting system of the IFAS structure relative to the conventional structure, including reduced shear wall base rotation, shear wall and column inter-story drift, and, in some cases, floor accelerations. These results indicate the potential for the IFAS to minimize damage to the primary structural and non-structural components during earthquakes.

## KEYWORDS

earthquake engineering, floor isolation system, inertial force limiting, low-damage system, seismic response reduction, shake-table testing

## 1 | INTRODUCTION

An innovative floor connecting system, termed the Inertial Force-Limiting Floor Anchorage System (IFAS), is described in this paper. The IFAS is intended to reduce horizontal inertial forces in building structures during major earthquakes.<sup>1,2</sup> This goal is accomplished by providing an engineered deformable connection as the primary connection

between the floor diaphragm and the vertical elements of the Lateral Force-Resisting System (LFRS). The LFRS elements (eg, structural walls, braced frames, etc.) resist lateral forces such as wind or earthquakes. The deformable connection unites the LFRS with the floor system and supporting columns that form the Gravity Load Resisting System (GLRS). The GLRS carries the gravity loads to the foundation.

In conventional design, stiff and strong diaphragm-to-LFRS anchorages are provided to create an essentially rigid connection between the LFRS and GLRS. The IFAS deformable connection, instead, possesses a lower strength than that required by the current design approach.<sup>3</sup> The connection will deform inelastically at this lower strength, transforming the excess diaphragm inertial force demands into lateral displacement of the floor system and attached GLRS relative to the primary vertical elements of the LFRS. This relative displacement also allows the IFAS to dissipate part of the earthquake energy in the building structure. The IFAS has the potential to limit the horizontal floor accelerations and to also reduce the seismic demands on the LFRS, actions that could potentially result in less damage to the structural and non-structural elements.<sup>2,4</sup>

This paper presents an examination of IFAS performance in a shaking table test program conducted at the Large High-Performance Outdoor Shake-Table at the NEES@UCSD experimental facility. The test structure was a 4-story partially precast concrete building structure built at half-scale (Figure 1). The structure was purposely designed with an eccentric wall layout relative to the unidirectional shake-table motion in order to examine the system performance of an IFAS deployed in both horizontal directions under longitudinal-torsional coupled response. A prototype IFAS system was developed for the shake-table testing using state-of-the-art components.<sup>4</sup> The IFAS prototype design used in the testing was optimized through extensive analytical research.<sup>1</sup>

The test program consisted of 3 phases that compared the IFAS performance to that of different conventional structural conditions. In order to meet the time and budget allotted for the project, the entire program was performed on a single test structure modified for each phase. In Phase I, the specimen with the newly proposed anchorage system was tested, termed herein *IFAS structure*; In Phase II, the floors were “locked” down to the walls to simulate a conventional floor anchorage in order to provide a direct comparison with Phase I, termed herein *conventional structure*. It is noted that the test building was designed with precast rocking walls to promote repeatability in structure performance, and thus the term “conventional” refers to the use of a stiff and strong anchorage between the floors and LFRS, as would occur in a conventional structure. In Phase III, the walls were “locked” into the foundations to simulate a reinforced concrete shear wall structure with higher strength to compare the response of a conventional structure with a stiffer, stronger LFRS, termed herein *strong structure*. The specimen was subjected to 22 strong ground motions. This paper presents the details of the shake-table testing program, focusing on the comparison of performance for structures with the IFAS system to that for structures with conventional floor anchorages. This information is presented primarily through the more direct comparison available between Phases I and II. Some limited observations are made relative to Phase III, which provides a baseline response for the rocking wall structure relative to a higher strength fixed-base wall.

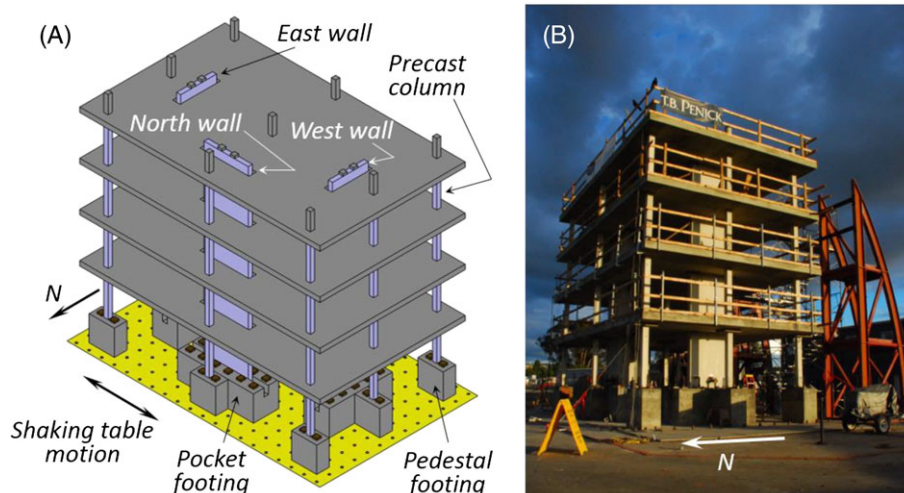


**FIGURE 1** Test structure: A, isometric model view; B, view from northwest [Colour figure can be viewed at [wileyonlinelibrary.com](http://wileyonlinelibrary.com)]

## 2 | INERTIAL FORCE-LIMITING ANCHORAGE SYSTEM (IFAS)

The IFAS builds on previous work on similar concepts discussed by Skinner et al, Key, Luco and De Barros, and Mar and Tipping<sup>5-8</sup> and most recently Crane.<sup>9</sup> The latter conducted shake-table tests on two small-scale 6-story specimens, one conventional and one with metal dampers between the floors and LFRS. A summary of these efforts appears in Tsampras et al.<sup>4</sup>

### 2.1 | IFAS concept

The concept of the IFAS is to partially uncouple the GLRS and LFRS seismic response through an engineered deformable connection between the two systems. Under wind and low seismic load, the IFAS is intended to transfer diaphragm forces to the LFRS similar to the essentially rigid connections in a conventional structure. However, under strong earthquake input, the connection reaches its predefined strength and deforms, thereby limiting the inertial forces in the GLRS. The idea of partially uncoupling the GLRS is attractive because most of the building mass resides there, and thus by limiting the force transfer, the IFAS has the potential to decrease seismic demands. The IFAS system has the potential to: (1) limit building horizontal inertial forces, thereby resulting in lower structural damage; (2) reduce floor accelerations, leading to less damage to acceleration sensitive non-structural elements and equipment<sup>10</sup>; and, (3) limit higher mode effects which induce large story shears in the LFRS and high forces in the diaphragm,<sup>11</sup> thus mitigating damage associated with these actions.

A tradeoff associated with the IFAS is that the force reduction is accompanied by relative displacement between the floor system (and hence the GLRS) and the vertical LFRS elements. This relative displacement must be limited in order to: (1) be practical from an architectural and building mechanical system standpoint; and (2) ensure a stable GLRS that does not undergo excessive inter-story drifts.<sup>12</sup> In the development of the concept, more aggressive designs (ie, a lower IFAS strength) that could greatly minimize the demand under the Design Basis Earthquake (DBE) were found to be feasible only if the larger relative displacement associated with this design could be limited under the Maximum Considered Earthquake (MCE) by re-engaging the floor.<sup>1</sup>

Conceptual IFAS designs were devised for different structural configurations including apartment buildings, office towers, and parking structures, and for different construction, eg, reinforced concrete, structural steel, and precast concrete.<sup>12</sup> These designs possess 3 main components, each of which acts between the floor system and primary elements of the vertical LFRS (eg, structural walls, braced frames, etc.): (1) force-limiting components to limit the inertial forces in the floor system and dissipate energy through inelastic deformation; (2) elastic restoring elements to minimize residual relative displacement between the floor system and LFRS, and also to brace the LFRS elements; and (3) re-engagement devices to limit the relative displacement and potential impact forces between the floor system and LFRS, necessary for more aggressive (lower strength) designs.

### 2.2 | IFAS prototype

An IFAS prototype was developed after a careful review of candidate state-of-the-art components and discussions with seismic design consultants.<sup>4,12</sup> The IFAS prototype is intended for application in reinforced concrete flat plate shear wall structures and consists of: (1) friction dampers (FD) or buckling-restrained braces (BRB) for the force-limiting components; (2) rubber bearings (RB) for the elastic restoring and LFRS stabilizing elements; and, (3) polyurethane bumpers, to limit the relative displacement of the floor to the wall. It is noted that the IFAS prototype system is composed of “off-the-shelf” devices developed for other applications that are effective in meeting the IFAS performance requirements, including the FD, originally proposed as a high-energy-dissipating diagonal bracing element<sup>13,14</sup>; the BRB, developed and used extensively as a ductile diagonal bracing element<sup>15,16</sup>; the RB, used extensively in bridge and other applications<sup>17</sup> due to its large shear deformation capacity; and the bumper, used effectively in automotive as well as other fields.<sup>18</sup>

Figure 2A, a section through the shake-table test specimen at the wall-floor interface, shows the IFAS prototype incorporated in the shake-table test structure. The IFAS force-limiting component was installed underneath the floor (in actual applications it can be located within a pocket in the slab) and is connected between the wall and the slab using spherical bearings (the FD is shown in Figure 2A; the specimen also contained BRBs). A moat is required between the shear-wall and the floor slab in order to accommodate the relative displacement (see Figure 2B). The moat creates an unbraced condition for the wall out-of-plane response. Thus, the RBs, in addition to providing an elastic restoring force to the floor system, also brace the wall at each floor level for out-of-plane stability by virtue of their position

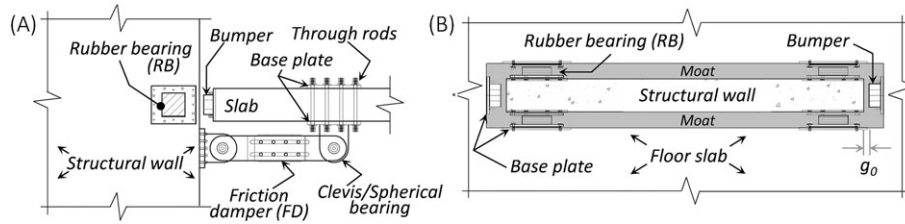


**FIGURE 2** IFAS prototype for shake-table test (EW direction): A, elevation; B, plan view

between the wall and the slab within the moat. The bumpers were installed on the slab within the moat at each end of the wall (Figure 2B). An initial gap,  $g_0$ , is provided between the bumper and the wall corresponding to the maximum allowable relative displacement desired between the wall and the floor.

It is noted that a cantilever slab condition was selected for the IFAS prototype rather than supporting the free slab edge on a ledge on the wall, based on analyses showing difficulty in controlling the critical friction forces under variable normal forces between the slab and the ledge.<sup>19</sup> This configuration was also conducive for the shake-table specimen construction where precast rocking walls were inserted into slots in the floor.

### 2.3 | IFAS feasible design space

A feasible design space for the IFAS prototype was developed through a series of parametric analyses.<sup>2,4,19</sup> The analytical studies were performed on a regular reinforced concrete shear-wall flat-plate apartment building that serves as an evaluation structure. Figure 3 shows the plan view of the building. It is important to note that the approach taken to develop the IFAS design space was to introduce the IFAS into an otherwise conventionally designed structure with the intent of lowering its demands, rather than modifying the design of the structure relative to current code in anticipation of any expected response reductions.<sup>12</sup> Thus, other than its floor anchorage, the evaluation structure design follows the equivalent lateral force (ELF) procedure of ASCE 7.<sup>3</sup> Further, because the IFAS is initially stiff prior to reaching its predefined strength, the building's elastic fundamental period, and hence its design forces, should not significantly differ from a conventional counterpart.

The studies examined structural performance versus IFAS strength via 2D nonlinear time-history analyses using a suite of design spectrum<sup>3</sup> compatible earthquakes for 4-, 8-, and 12-story buildings. The building models possessed idealized models for the IFAS devices with similar hysteretic characteristics to the eventual IFAS prototype.<sup>2,4</sup> Figure 4 shows representative analytical results for the 4-story evaluation structure: (A) LFRS and GLRS inter-story drift ratio; (B) relative displacement between the LFRS and floor; and (C) floor acceleration. Averaged maximum response under the DBE and MCE level are indicated by black and gray curves, respectively.

The parameter displayed on the horizontal axis,  $\alpha$ , is the IFAS strength normalized by the current code diaphragm design force  $F_{px}$ ,<sup>3</sup>  $\alpha = \Sigma F_y / F_{px}$ , where  $\Sigma F_y$  is the total strength of the IFAS in one (lateral) direction for each floor. Note that because the diaphragm connection is part of the collector system, the application of the system overstrength factor  $\Omega_o$  and strength reduction factor  $\phi$  in the design of diaphragm collectors leads to a current code nominal strength  $\alpha$  value for a conventional structure not of unity, instead  $\alpha = \Omega_o / \phi = 3.33$ . Thus, the range shown in Figure 4 are all

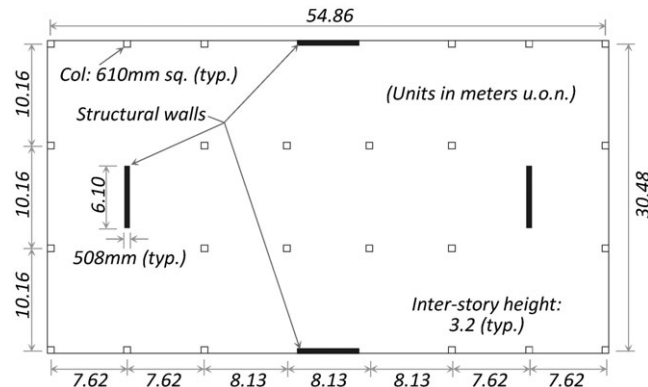


**FIGURE 3** Evaluation structure plan view

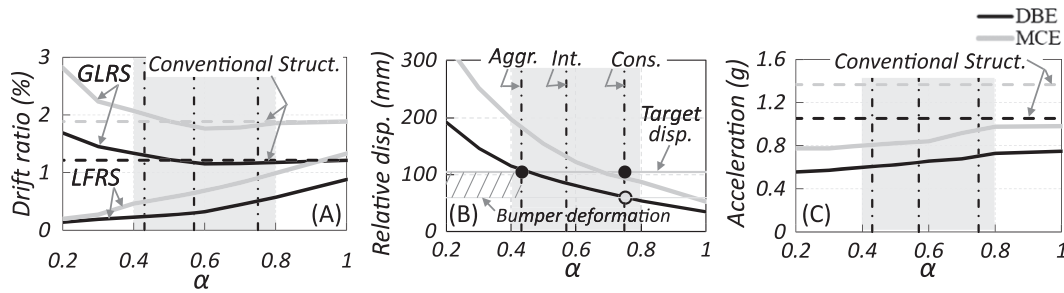


**FIGURE 4** IFAS design space: A, inter-story drift ratio; B, LFRS-to-floor relative displacement; C, floor acceleration

deliberately weaker designs than that in a conventional structure. Note that  $\alpha = 0$  (not shown) represents an ideal fully isolated floor system. As seen, LFRS drift and floor acceleration decrease as the IFAS strength decreases, while GLRS drift and relative displacement increase. For reference, the conventional structure responses ( $\alpha \geq 3.33$ ) for drift and acceleration are shown as dashed horizontal trend lines in Figure 4A,C. Figure 4B shows the full-scale target displacement limit (100 mm) selected for the prototype.<sup>4</sup>

The gray shaded regions in Figure 4 represent the feasible domain for the IFAS identified in the analyses. In this design space, LFRS drift ratio and floor acceleration response are reduced relative to a conventional structure, yet LFRS-to-floor relative displacement and GLRS drift response fall within acceptable limits. Thus, the analytical results provide a range of appropriate seismic capacities for the IFAS relative to current diaphragm design force.

Two IFAS strength levels at each end of this space are noted: (1) a “conservative” design, defined by where the floor relative displacement reaches the target displacement in the MCE, resulting in more modest reduction of LFRS drift ratio and floor acceleration; and (2) an “aggressive” design, where the floor relative displacement reaches the target displacement in the DBE, resulting in more significant reduction in LFRS drift ratio and floor acceleration. In order to prevent excessive relative displacement and GLRS drift in the MCE, an aggressive design requires the introduction of re-engagement devices. Thus, a conservative design is able to limit floor relative displacement and GLRS drift ratio in the MCE through its inherent strength, while an aggressive design relies on the bumper element to limit these actions in the MCE, thereby permitting more significant DBE response reduction. The range of bumper engagement, initiating from the conservative design DBE displacement, is shown in Figure 4B.

For the shake-table test specimen design (presented in Section 3.6), the feasible design space was used in lieu of a formal IFAS design procedure which will be a future outcome of this work. The IFAS design strengths selected for the test building are indicated by vertical trend lines in Figure 4: (1)  $\alpha = 0.75$ , is reflective of a “conservative” design; (2)  $\alpha = 0.44$ , representing an “aggressive” design; and (3)  $\alpha = 0.57$ , representing an “intermediate” design.

### 3 | PROOF OF CONCEPT

#### 3.1 | Test facility

Proof-of-concept testing was performed on the 12.2 m long by 7.6 m wide 6.8MN capacity unidirectional outdoor shake-table of the University of California, San Diego, formerly known as NEES@UCSD.<sup>20</sup>

#### 3.2 | Shake-table specimen overview

The relatively large floor plan of the evaluation structure used to define the feasible design space (Figure 3) made it impossible to build a large-scale model of this building on the NEES@UCSD shake-table platen. A half-scale 4-story test structure with a large plan eccentricity was chosen as the best alternative to conduct a proof of concept test. In this structure, lateral resistance in two orthogonal directions is provided by structural walls (Figure 5A). The wall acting in the EW direction (termed herein North Wall) is offset northward from the floor center of mass (COM) by 2.13 m to purposely create an eccentric LFRS layout in the direction of the table motion. This eccentricity produces a strong coupled lateral-torsional response, allowing: (1) the simultaneous evaluation of different IFAS devices (FDs and BRBs) in each direction; and, (2) the ability to observe IFAS performance under the complex kinematics of a torsionally sensitive structure. The eccentric wall layout makes these actions possible on the unidirectional NEES@UCSD shake-table.

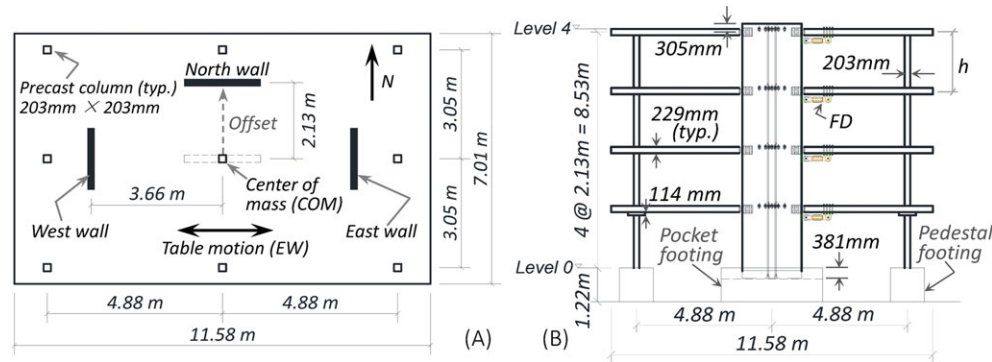


**FIGURE 5** Shake-table test structure: A, plan view; B, elevation (north view) [Colour figure can be viewed at [wileyonlinelibrary.com](http://wileyonlinelibrary.com)]

The transverse walls, identified as the East and West Walls, acting in the NS direction flank the COM by 3.66 m. To maximize the floor footprint for the shake-table platen tie-down layout, the column locations were moved slightly inward from the perimeter.

Figure 5B shows the test structure elevation. A floor-to-floor height  $h = 2.13$  m was selected for the shake-table test structure in order to provide sufficient overhead clearance for construction workers and researchers (corresponding to  $h = 4.27$  m for a full-scale prototype). The structure was erected on pedestal footings, with walls placed in pockets for the purpose of enabling the emulation<sup>21</sup> of a cast-in-place shear wall in Phase III testing.

A key objective of the shake-table test program was to directly compare the IFAS structure (Phase I) to an analogous conventional structure (Phase II). Thus, test repeatability was paramount. For this reason, the test structure utilized post-tensioned precast hybrid rocking (PT) walls,<sup>22-24</sup> instead of the more common fixed-base reinforced concrete shear-walls, as rocking walls tend to degrade less rapidly, and thus allow a more valid comparison between the phases. This approach has been used successfully in previous shake-table testing.<sup>25</sup> It should be noted that the use of the proposed IFAS system does not require the additional use of PT walls.

Figure 6 shows the typical wall detail. The precast wall units were single full-height (9.22 m), 203-mm-thick elements. The walls employed unbonded post tensioned (PT) bars for self-centering and special energy dissipator (ED) devices<sup>26</sup> for supplemental dissipation (Figure 6D). Rubber bearing pads under the PT bar nuts extended the wall elastic drift range. The wall unit included embedded steel plates for the IFAS devices and embedded slots for the PSA slotted inserts (described subsequently) used in Phase II (Figure 6A,B). A steel channel served as the wall base for good confinement and toe armor (Figure 6C). Steel beads welded to the bottom surface of the steel channel provide sliding resistance between the wall and footing. A layer of 13-mm grout was placed at the bottom of the pockets to provide a level surface at the PT wall base and provide sliding resistance in combination with the steel beads. Differences in the North and transverse wall designs appear in the Figure 6 table inset.

In Phase III, a portion of the pocket extending beyond the wall length 76.2 mm on either end was filled with commercially available non-shrink, metallic aggregate grout (Embeco\* 885); the remainder of the pocket was filled with concrete. This step created a precast “emulative” fixed-base wall with high strength (ASTM A1035 grade-100) longitudinal reinforcement. The grout was mixed to flowable consistency in multiple batches using a hand-held grout mixer, half a bag (12.3 kg) of grout per batch; 50 mm × 100 mm cylinder samples were taken and tested, with minimum/average 5-day grout strengths of 53 MPa/60 MPa on the day of Phase III testing (Table 2).

The test structure was constructed with cast-in-place RC floor slabs. The slab thickness was not scaled (rather than adding mass) to provide sufficient tributary mass to develop realistic diaphragm forces; a more realistic relationship between gravity load, P-Δ effects, and inertial forces, and, to keep the table accelerations within the operating range.<sup>20</sup> The larger relative thickness of the slab creates a condition where it is difficult to enforce a strong column-weak slab design condition to preclude a story mechanism. For this reason, and for test repeatability, special precast concrete gravity columns (Figure 7) were developed for the structure. These columns are intended for less damage and larger drift capacity in comparison to the typical cast-in-place RC columns used in flat-plate construction. The precast column section was 203-mm square and had a central corrugated metal duct on one end and a central #7 ASTM A1035 grade-100

\*BASF. <https://www.master-builders-solutions.basf.us/en-us/products/masterflow/1715>.

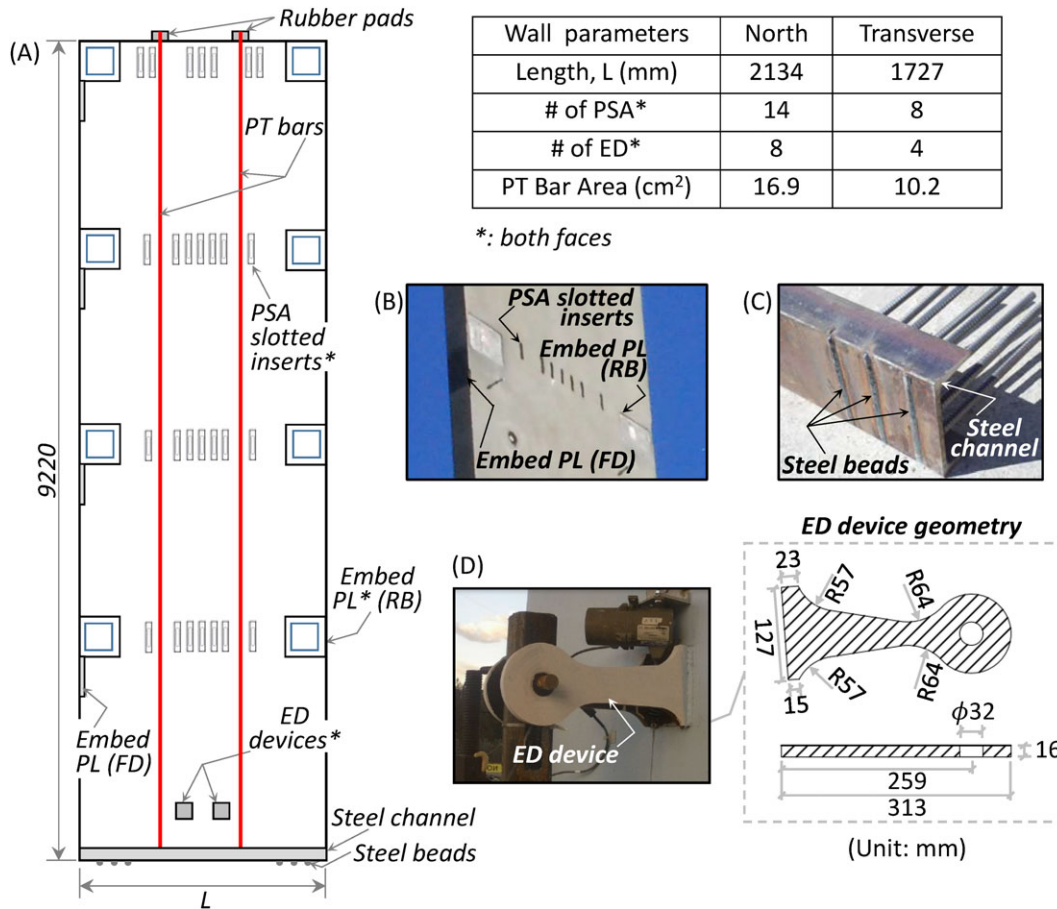


FIGURE 6 North wall detail: A, wall; B, embedded plates; C, steel channel; D, ED device [Colour figure can be viewed at wileyonlinelibrary.com]

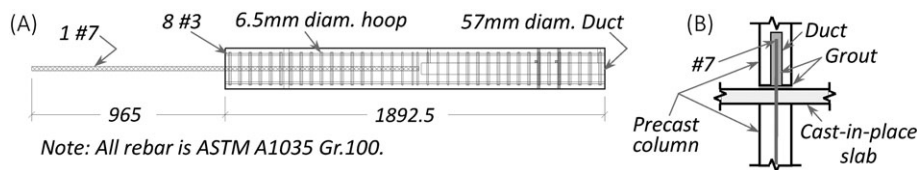


FIGURE 7 Precast column: A, reinforcing detail; B, column joint detail (units: mm)

high strength reinforcing bar extending from the other end (Figure 7A). Figure 7B shows a schematic drawing of the column-slab interface detail. The slab was cast above the lower story column, bonding to the upward protruding bar. The next tier of columns was then slipped over the protruding bar, and the duct and base interface was filled with high-strength shrinkage compensating proprietary grout.

Concrete and grout cylinder tests were conducted several times during construction and testing. The measured material properties (averaged over the number of tests, *n*) at the beginning of testing (except as noted) are reported in Tables 1 and 2. Reinforcement tensile test results (average values of 2 coupon tests) are shown in Table 3.

TABLE 1 Concrete cylinder test (units: MPa for *f<sub>c</sub>* and *E<sub>c</sub>*)

Flr. 1 Column			North Wall			Transverse Wall			Slab			Footing		
<i>f<sub>c</sub></i>	<i>E<sub>c</sub></i>	<i>n</i>	<i>f<sub>c</sub></i>	<i>E<sub>c</sub></i>	<i>n</i>	<i>f<sub>c</sub></i>	<i>E<sub>c</sub></i>	<i>n</i>	<i>f<sub>c</sub></i>	<i>E<sub>c</sub></i>	<i>n</i>	<i>f<sub>c</sub></i>	<i>E<sub>c</sub></i>	<i>n</i>
42	23 215	3	52	24 534	3	66	26 022	6	54	22 189	12	50	25 403	9



**TABLE 2** Grout cylinder test (units: MPa for  $f'_c$ )

Flr. 1 Column		Flr. 2 Column		Flr. 3 Column		Flr. 4 Column		Wall Base		Footings Pockets (Phase III)	
$f'_c$	$n$	$f'_c$	$n$	$f'_c$	$n$	$f'_c$	$n$	$f'_c$	$n$	$f'_c$	$n$
69	3	72	3	71	3	73	3	84	3	60	5

**TABLE 3** Reinforcement tests (units: MPa for  $f_y, f_u, E_s$ )<sup>a</sup>

Grade	Size	Specified $f_y$	Measured $f_y$	$E_s$	Measured $f_u$	Strain at $f_u$	Location
G60	No. 3	414	516	181 602	770	0.1094	Slab
G100	No. 2	689	924	174 981	1171	0.0496	Confining reinforcement in walls and columns
G100	No. 4	689	899	192 112	1163	0.0525	Footings and walls
G100	No. 7	689	1016	163 643	1478	0.0636	Columns

<sup>a</sup> $f_y$  is the yield strength, measured at 0.2% offset strain;  $f_u$  represents maximum measured stress. Bars are longitudinal u.o.n.

### 3.3 | IFAS prototype for shake-table specimen

The force-limiting components used for the shake-table specimen are FDs and BRBs (Figure 8). These elements were selected, after careful review of many candidate devices<sup>4</sup> and full-scale testing,<sup>27,28</sup> to provide the stable hysteretic energy dissipation, deformation capacity, and controllable strength required of the IFAS.

The FD assembly<sup>27</sup> involved (Figure 8A): (1) clamped steel plates, consisting of a slotted internal sliding plate and 2 fixed external plates; (2) 8 friction bolts (A325, 19-mm diameter) with lubricated bushings to reduce friction on the slots and Belleville washers for even preload; (3) a pair of thin AFT-200<sup>†</sup> composite shim plates between the internal and external plates to better control the FD slip force; and (4) guiding plates to prevent rotation. The FD strength is easily adjusted by changing the bolt pretension force. The FD design deformation limit was 63.5 mm. The FDs were installed using spherical bearings for articulation in the asymmetrical structure.

As opposed to the off-the shelf BRB<sup>‡</sup> used in the full-scale testing,<sup>28</sup> the half-scale BRB was custom-made,<sup>29</sup> consisting of (Figure 8B): (1) a milled steel bar with 8 small reduced-diameter yielding segments to dissipate energy under cyclic loading; (2) an inner steel pipe providing the contact surface for the lubricated larger-diameter regions of the milled bar; (3) an outer steel pipe for the outside surface; and (4) grout between the inner and outer pipes to provide sufficient stiffness and prevent buckling under compression. The BRBs employed pinned clevises on both ends. Steel material properties for the BRB and FD, along with the PT and ED, appear in Table 4. The grout used for the BRB is similar to that in Table 2.

The RBs<sup>§</sup> were carbon fiber square bearings with 7 laminations (Table 5). The RBs were epoxied to two end steel plates (Figure 9B) with ground surfaces for better adhesion. The RBs were installed by welding one steel plate to the wall embed plates and bolting the other steel plate to embed plates in the floor slab (Figure 9A). The RBs were placed at 4 locations on each shear wall at each floor level as shown in Figure 2A.

The polyurethane bumpers<sup>¶</sup> were pre-attached using set screws to a steel base plate with a steel ring (Figure 9C). The steel base plate was in turn installed on the slab using threaded rods (Figure 9A). The steel ring provides confinement for the bumper to permit a gradually increasing resistance to prevent high impact forces. The bumper nominal deformation capacity is  $\delta_b = 19.5 \text{ mm}$ <sup>19</sup> and were installed with  $g_0 = 30.5 \text{ mm}$  (Figure 2B), permitting the slabs to reach their intended half-scale target displacement of 50 mm with respect to the LFRS.

<sup>†</sup>Champion Technologies, Inc. <http://www.stillchampion.com/aft-200.html>.

<sup>‡</sup>Star Seismic. 6300 N Sagewood Dr, Park City, UT 84098.

<sup>§</sup>DYMAT<sup>™</sup> Construction Products, Inc. PO Box 834, Solana Beach, California 92075.

<sup>¶</sup>Pleiger Plastics Company. PO Box 1271-498 Crile Road Washington, PA, 15301-1271.

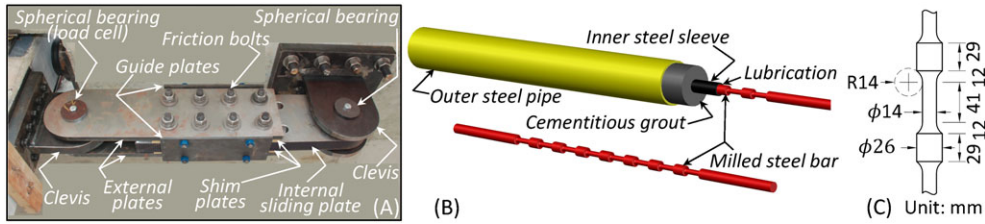


**FIGURE 8** Force-limiting component detail: A, annotated FD photo; BRB: B, schematic; C, milled steel bar detail [Colour figure can be viewed at wileyonlinelibrary.com]

**TABLE 4** Steel material properties (units: MPa for strength)

Device	Component	Yield Strength	Tensile/Ultimate Strength	Elongation, %
FD <sup>a</sup>	Clamped steel plates	345	450	≥ 21
BRB <sup>a</sup>	Milled steel bar	310	462	≥ 36
	Steel pipe/sleeve	240	415	≥ 30
ED <sup>b</sup>	Steel plate	432–447	568–578	23–24
PT bar	North wall <sup>b</sup>	862	1075.6	≥ 6
	Transverse wall <sup>c</sup>	931	1103.2	≥ 6

<sup>a</sup>Nominal values.

<sup>b</sup>Manufacturer values.

<sup>c</sup>Coupon tests of same material from different heat.

**TABLE 5** Carbon fiber RB properties (half-scale)

Direction	Dimension, mm	Shear Modulus, kN/mm <sup>2</sup>	Layer Thickness, mm	No. of Layers	Shape Factor	RB Stiffness, kN/mm
EW	178	$6.55 \times 10^{(-4)}$	6.4	8	7	0.41
NS	152	$6.55 \times 10^{(-4)}$	6.4	8	6	0.30

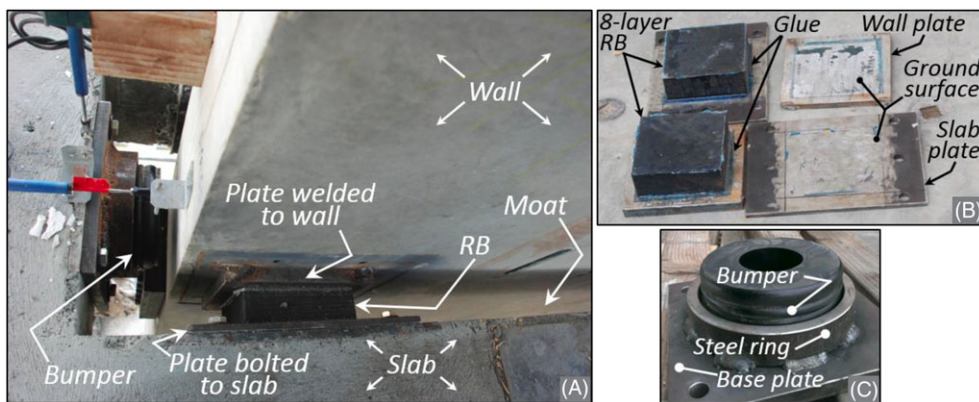


**FIGURE 9** Restoring and displacement-limiting devices: A, layout; B, RB assembly; C, bumper [Colour figure can be viewed at wileyonlinelibrary.com]

### 3.4 | Floor anchorage layouts: IFAS vs conventional

The primary difference between the Phase I and later structures is the manner in which the GLRS is attached to the LFRS. The shake-table test specimen had to be designed to allow modification of the floor anchorage connection from the IFAS in Phase I to one simulating a conventional floor anchorage (eg, dowel bars that provide a highly stiff and strong connection) for Phases II and III. This objective was complicated by the presence of the moat required for the IFAS. The IFAS floor anchorage details and the manner in which the structure was converted to simulate a conventional anchorage is now presented. The anchorage properties are provided later in Section 3.5.

Figure 10A shows a typical floor of the test specimen during Phase I. The location of the IFAS devices is indicated on the underside of the upper floor shown (refer to Figures 8 and 9 for detail views of these devices). Note the FDs are attached to the North wall parallel to the table motion and BRBs are attached to the transverse walls.

The location of the anchorages devices subsequently connected for Phases II and III are indicated on the lower floor visible in Figure 10A. A special steel anchorage device, the PSA,<sup>#</sup> was used to connect the floors to the walls to simulate the conventional structure. The PSA involves threaded dowels (“strap anchors”) that are inserted into spring-loaded nuts that ride in vertical slots (“inserts”) precast into the wall elements. The connection is completed by welding the flat end of the threaded rods to embed plates in the slab. The PSA transfers horizontal forces from the slab to the wall but permits relative vertical movement of the wall with respect to the slab. This feature is crucial for the test specimen rocking walls, due to the relatively short spans to adjacent columns on the platen.

Figure 10B shows the fully completed PSAs on the North wall (7 on each face, at each level) and transverse wall (4 on each face, at each level). Standard PSA 50.8 mm × 9.53 mm straps were used with 6035 inserts<sup>15</sup>. The PSA strength and stiffness depend on the free span length of the strap between the wall face and floor weld. A nominal design eccentricity of 50.8 mm was chosen resulting in a design strength of 63.2 kN and a design stiffness of 8.58 kN/mm.

The PSA configuration was found to not produce a completely rigid anchorage. Thus, tight-fitting roller bearings (Figure 10C) were introduced in the moat region between the North wall end and slab for the final two Phase II and all Phase III tests. These bearings provided a direct load transfer to the wall, thereby supplementing the PSA horizontal stiffness. It is also noted that the FDs and BRBs were left in place for the first three Phase II tests.

### 3.5 | Shake-table specimen design

The shake-table test prototype structure was designed for a Seismic Design Category E site<sup>3</sup> in downtown Berkeley, California (BE). The PT walls used for the test specimen were designed using displacement-based methods.<sup>24,29</sup> It should be noted that displacement-based design is not required for use of the IFAS. Figure 11A shows the pushover analysis results for the North wall.<sup>19</sup> Indicated on the curve are the yield and ultimate strength of the PT walls ( $M_y$ ,  $M_{0.03}$ ), defined as the wall strength at 0.5% and 3% roof (wall tip) drift ratio, normalized by the required strength  $M_u$ . Note that the transverse wall design strength (not shown) is approximately half that of the North wall because there are two transverse walls in the NS direction.

It is useful to examine the structure in the context of an ELF design because the IFAS strength index  $\alpha$  is based on  $F_{px}$ . Accordingly, a horizontal trend line is shown in Figure 11A for the required design strength of the BE site ( $M_u = 3106$  kN-m) for the analogous ELF design, based on  $R = 6$  for Special RC Shear Walls.<sup>3</sup> The required design strength ( $M_u = 2359$  kN-m) for a Seismic Design Category D design in Seattle, WA (SE) is also indicated in the figure.

It is important to note that, other than the differences in floor anchorage strength, the Phase I and II structures are intended to possess the same design lateral stiffness and strength. However, some degradation of the structure during testing is unavoidable. In this regard, another advantage of using PT walls is that the test structure lateral strength is adjustable based on the level of initial prestress in the PT bars. Table 6 shows the North wall strengths targeted in the test program, expressed as a ratio of the required strength, at yield ( $M_y/M_u$ ) and ultimate ( $M_{0.03}/M_u$ ) for the BE and SE sites. The initial prestress level is expressed as a percentage of bar ultimate strength ( $F_{ult}$ ), ie,  $\rho = 0.4$  represents 40% $F_{ult}$ . Table 6 indicates wall yield strength increases as  $\rho$  increases. It is noted that the BE design is based on  $\rho = 0.6$ . The fixed-base Phase III shear wall is also included in Table 6 and Figure 11B.

<sup>#</sup>JVI Inc. 7131 North Ridgeway Ave Lincolnwood, IL 60712.

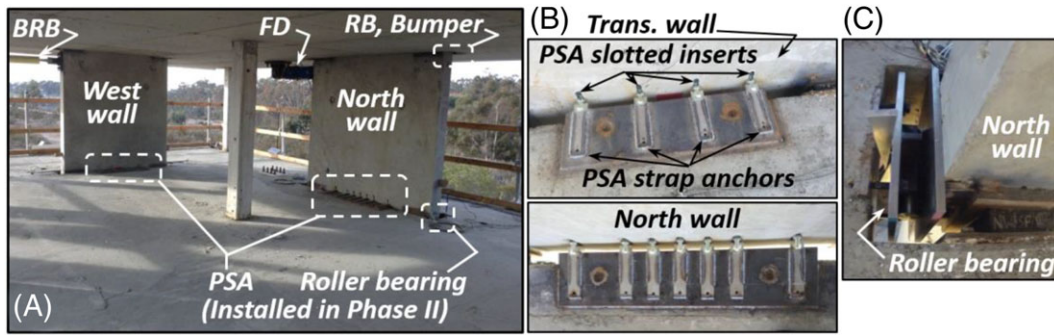


**FIGURE 10** Floor anchorages for typical floor: A, device locations; B, PSA; C, roller bearing [Colour figure can be viewed at wileyonlinelibrary.com]

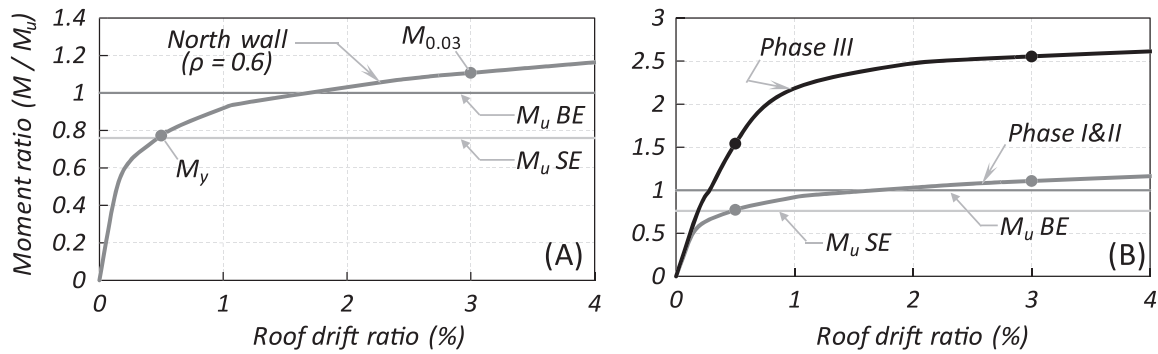


**FIGURE 11** North wall design capacity: A, relative to design strength (for BE site); B, phase III comparison

**TABLE 6** North wall property (half-scale structure)

Wall Strength	$M_y/M_u$		$M_{0.03}/M_u$	
	BE	SE	BE	SE
$\rho = 0.4$	0.59	0.77	1.04	1.38
$\rho = 0.5$	0.68	0.90	1.09	1.43
$\rho = 0.6$	0.77	1.02	1.11	1.46
$\rho = 0.7$	0.86	1.13	1.12	1.47
Phase III	1.54	-	2.55	-

### 3.6 | Test specimen IFAS design

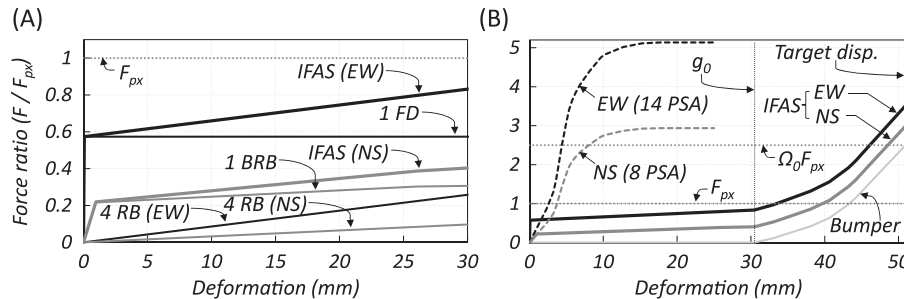
The IFAS nominal design strength was selected to correspond to the levels indicated in Figure 4B. For the BE site diaphragm design force  $F_{px} = 194$  kN, the intermediate ( $\alpha = 0.57$ ) and aggressive ( $\alpha = 0.44$ ) designs result in IFAS limit strengths of 111 and 85 kN, respectively (Table 7). These values correspond to conservative ( $\alpha = 0.76$ ) and intermediate designs for the SE site with  $F_{px} = 147$  kN. Note that the different design strengths are possible in the EW direction due to the adjustability of bolt pretension in the FD. The BRBs are not adjustable; thus, a single strength, 42.5 kN, for two devices per floor in the NS direction, translates into  $\alpha$  values of 0.44 (aggr.) / 0.58 (int.) for the BE/SE sites. A constant IFAS design strength pattern was used along the height of the structure.

Figure 12 shows the IFAS nominal strength as design backbone curves, showing the contribution of different components to system strength. Figure 12A shows the EW ( $\alpha = 0.57$  for BE Site) and NS IFAS characteristic over the deformation demand range expected in the DBE. As seen, the FD is expected to be much stiffer than the BRB in the elastic range. Thus, when a BRB is used, the IFAS may introduce a measure of flexibility under service load. The contribution of the RB at the IFAS limit strength is fairly negligible (see Table 7 note). However, this contribution, representing the

**TABLE 7** IFAS design (half-scale structure)

Direction	Site	$F_{px}$ , kN	$\alpha$	IFAS Limit Strength <sup>a</sup> , kN	RB Force @30.5 mm, kN	# RB	IFAS Strength @30.5 mm, kN
EW	BE	193.9	0.57	111.3	12.7	4	161.9
			0.44	84.6	9.6	123.1	
	SE	147.4	0.76	111.3	12.7	4	161.9
			0.57	84.6	9.6	123.1	
NS	BE	193.9	0.44	2@42.5	4.8	4	61.0
	SE	147.4	0.58	2@42.5	4.8	4	61.0

<sup>a</sup>Includes RB force at force-limiting component strength: 0.1 kN for FD; 0.6 kN for BRB.

**FIGURE 12** IFAS backbone characteristic curves (at half-scale) targeted for: A, DBE; B, MCE, at the BE site

elastic restoring force of the system, becomes important at the anticipated relative displacement in the DBE. This displacement (open circle in Figure 4B) is aligned to the bumper gap,  $g_0$ , resulting in a value of 30.5 mm at half scale. Figure 12B shows the IFAS characteristics extended to the MCE target displacement (50 mm at half-scale). As seen, the bumper picks up force at an ever increasing rate, arresting the relative displacement between the floor and LFRS. Note that the NS-direction PSA is total per individual transverse wall.

### 3.7 | Test structure: Scaling and summary of specific characteristics

The test structure is built at half scale. Thus, all full-scale dimensions are halved, with the exception of slab thickness, as mentioned previously. The ground motion was compressed in time with a factor  $1/\sqrt{2}$ ; its acceleration magnitude was not scaled because of the unscaled slab thickness. The scale factors of various structural responses presented in the paper are given in Table 8. These factors match the Cauchy-Froude similitude law, which has general validity independent of the material nonlinearity.

In summary, in order to perform the full testing program on a single structure on a unidirectional shake-table, the test structure possessed the following aspects not directly related to the IFAS: (1) precast rocking walls; (2) an asymmetric LFRS layout in plan; (3) pinned-ended precast columns; and (4) PSA slotted inserts and roller bearings.

**TABLE 8** Scale factors for test specimen response

Structural Response	Scale Factor	Structural Response	Scale Factor
Floor acceleration	1:1	Relative displacement	1:2
LFRS and GLRS drift ratio	1:1 <sup>a</sup>	Slab twisting angle	1:1
Wall base rotation	1:1 <sup>a</sup>	Forces	1:4

<sup>a</sup>This scale factor holds for a full-scale prototype with floor-to-floor height  $h = 4.27$  m.

## 4 | SHAKE-TABLE TEST PROGRAM

### 4.1 | Test sequence

The shake-table test sequence, including Phase I: IFAS; Phase II: conventional; and Phase III: strong, is shown in Table 9. Test excitation involved: (1) low-amplitude white noise motions and (2) strong ground motions, representing DBE and MCE for the BE and SE sites. In addition, a BE service (SVC) record was performed to initiate some sequences at lower demand. The MCE and SVC amplitudes are obtained by scaling the DBE by 150% and 67%, respectively. The white noise (WN) motions were applied to the structure typically before and after each day's test protocol. Table 9 also includes the average measured wall PT ratio  $\rho$  and IFAS strength  $\alpha$ . Two  $\alpha$  values are listed for each test: the upper entry is the nominal design  $\alpha$ ; the lower entry is the average  $\alpha$  measured over the floors (for tests where this measurement was taken). Good control of FD strength is observed. The PSA nominal design strength<sup>30</sup> is used to calculate the nominal design  $\alpha$  for Phase II. Tests used for comparison in Section 5 are highlighted in gray. These tests were selected due to similar PT ratios in the Phase I and corresponding Phase II tests. Note that the applied PT force in the selected Phase II tests are higher than the Phase I (eg, tests 11 and 18), to achieve an essentially constant wall yield strength as the wall degraded, and provide a better comparison.<sup>19</sup>

### 4.2 | Ground motions

The structure was investigated under spectrum compatible DBE and MCE earthquakes corresponding to the Seattle (SE) and Berkeley (BE) sites. A different historic ground motion was selected and scaled for each site (Table 10\*\*). Note the records were applied in one direction (refer to Figure 1A). No vertical acceleration was applied.

Figure 13A,B shows the scaled (DBE level) time histories of the SE and BE earthquake records used in the shake-table test. The records were compressed in time by a factor of  $1/\sqrt{2}$  relative to the original records. Figure 13C shows the DBE-level response and design spectra. The analytically determined elastic structure first and second mode periods are denoted as  $T_1$  and  $T_2$ . The shaded regions represent the small period change between the IFAS and PSA structures.

### 4.3 | Instrumentation

Figure 14 provides the instrumentation layout in plan and elevation schematics summarizing the sensors used in the shake-table test. String potentiometers (pots) were deployed: (1) in X-shape configurations in the northwest and southeast perimeter bays at each story for measuring inter-story drift of the GLRS; (2) at two locations along the floor east perimeter at each floor level and connected on the other end to a fixed steel frame adjacent to the shake-table platen to measure absolute floor displacement in EW direction and floor twist in plan; (3) between the slab and the North wall at each level to measure floor relative displacement, attached at sufficient distance from the wall to minimize kinematic error due to wall uplift; and, (4) at the wall bases to measure wall uplift for base rotation calculations (in- and out-of-plane) and estimate the wall neutral axis for base moment calculations. Linear potentiometers were installed: (1) between the wall and the slab at each level to measure the uplift and horizontal relative displacement; (2) at selected first-story column top and bottom regions to measure column end rotations; (3) at the BRB and FD to measure device deformation; (4) in spring-loaded fashion to measure the roof bumper compressive deformation; and, (5) across the moat to capture PSA deformation. Accelerometers were installed: (1) on the shake-table platen and at the top of the foundations; (2) on each floor to measure the EW acceleration at A, B, C on line 1 and NS acceleration at 1 and 3 on line C (EW and NS accelerations were measured at each corner on the roof); and (3) on the south surface of the North wall to measure impact effect (starting after Test 10). Additionally, accelerometers measuring vertical acceleration were installed on floors 1 and 3.

PT force was measured using pressure transducers; FD force was measured using cylindrical bearing load cells; ED and BRB force was calculated using strain gage readings on components in series with those elements that remained elastic during the test. Strain gages were also attached to high strength reinforcement in the North wall and some

\*\*<http://ngawest2.berkeley.edu/>

**TABLE 9** Shake-table test sequence

TEST #	Motion Name	Intensity	$\rho$ (EW/NS)	$\alpha$ (EW)	TEST #	Motion Name	Intensity	$\rho$ (EW/NS)	$\alpha$ (EW)
Phase I									
1-W1	WN	0.03 g	0.61/0.60 <sup>a</sup>	0.27	1-W10	WN	0.03 g	0.60/0.66	0.44
Test 1	BE	SVC	0.61/0.60 <sup>a</sup>	-	Test 13	BE	DBE	0.60/0.66	0.44
1-W2	WN	0.03 g	0.61/0.43	0.24	Test 14	BE	MCE	0.59/0.65	0.43
Test 2	BE	SVC	0.61/0.43	0.44	1-W11	WN	0.03 g	0.56/0.65	0.44
Test 3	SE	DBE	0.61/0.43	0.45	2-W12	WN	0.03 g	0.64/0.71	4.56
Test 4	BE	DBE	0.61/0.42	0.44	Test 15	SE	DBE	0.64/0.71	6.00
1-W3	WN	0.03 g	0.61/0.42	0.45	Test 16	BE	SVC	0.63/0.70	4.56
1-W4	WN	0.03 g	0.49/0.41	-	Test 17	BE	DBE	0.64/0.71	4.56
Test 5	BE	SVC	0.49/0.42	0.57	2-W13	WN	0.03 g	0.59/0.71	4.56
Test 6	Seattle	DBE	0.49/0.41	0.61	2-W14	WN	0.03 g	0.64/0.64	PSA + roller bearing
Test 7	BE	DBE	0.49/0.41	0.57	Test 18	BE	DBE	0.64/0.63	
1-W5	WN	0.03 g	0.49/0.41	0.61	2-W15	WN	0.03 g	0.61/0.63	
1-W6	WN	0.03 g	0.50/0.42	-	Test 19	BE	MCE	0.60/0.62	
Test 8	BE	DBE	0.50/0.42	0.44	2-W16	WN	0.03 g	0.56/0.60	
				0.41					
Phase II									

(Continues)

TEST #	Motion Name	Intensity	$\rho$ (EW/NS)	$\alpha$ (EW)	TEST #	Motion Name	Intensity	$\rho$ (EW/NS)	$\alpha$ (EW)	
Test 9	Seattle	MCE	0.50/0.42	0.57	Phase III	3-W17	WN	0.03 g	0.46/0.70	
Test 10	BE	MCE	0.50/0.42	0.56		Test 20	BE	DBE	0.46/0.70	
1-W7	WN	0.03 g	0.42/0.42	0.44		3-W18	WN	0.03 g	0.45/0.70	
1-W8	WN	0.03 g	0.60/0.62	0.42		Test 21	BE	MCE	0.45/0.70	
Test 11	BE	DBE	0.59/0.62	0.44		Test 22	BE	MCE	0.47/0.70	
Test 12	BE	MCE	0.59/0.62	-		3-W19	WN	0.03 g	0.52/0.71	
1-W9	WN	0.03 g	0.53/0.62	0.57						
				0.56						
				0.57						
				-						
				0.57						
				0.55						
				0.57						
				0.56						

WN intensity is root mean square value.

<sup>a</sup>Indicates design PT ratio, accurate measurement not available.



TABLE 10 Earthquake records

Earthquake ID	Earthquake	Station	Component	Magnitude	Scale Factor	Scaled PGA, g
SE	1979 Imperial Valley	El Centro Array #5	140	6.5	1.14	0.59
BE	1989 Loma Prieta	LGPC	000	6.9	0.72	0.41

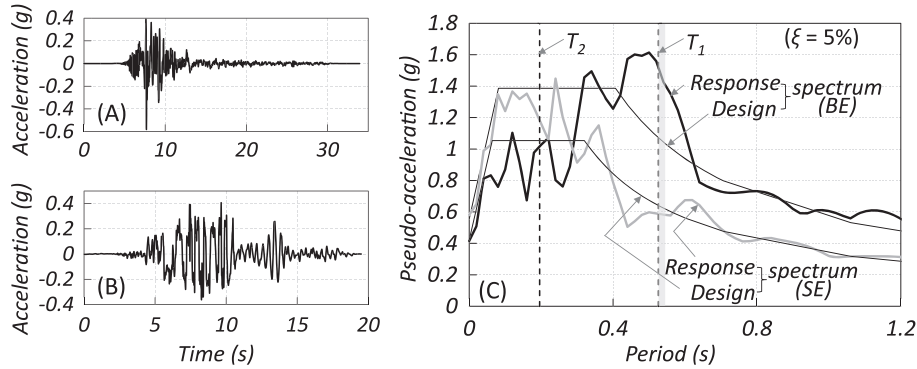


FIGURE 13 Test ground motions (scaled): A, SE time history; B, BE time history; C, response spectra

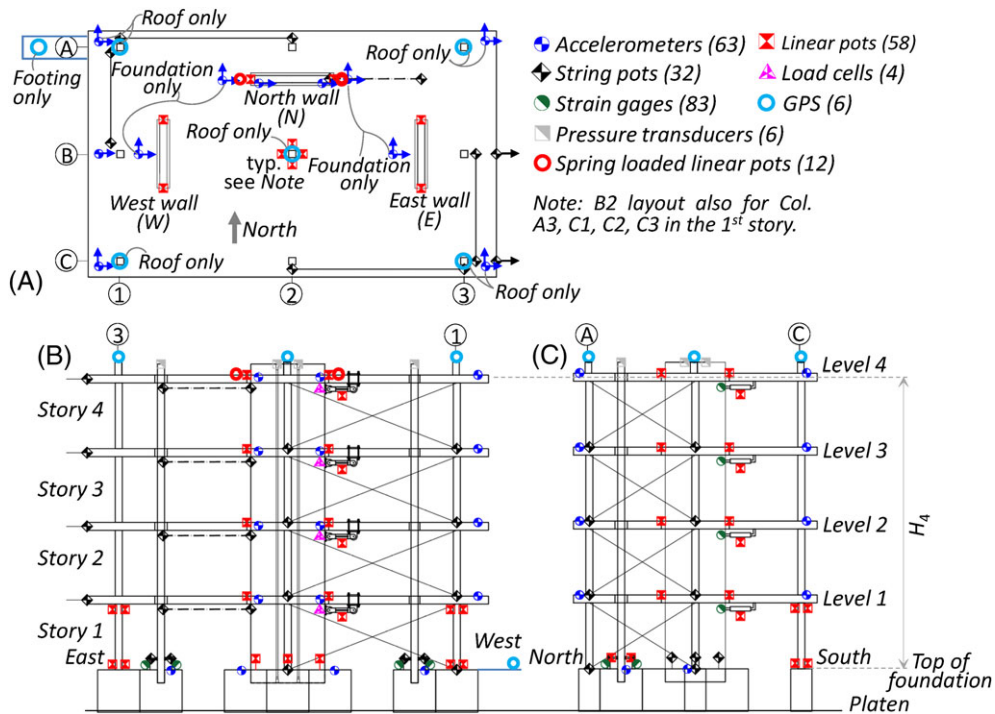


FIGURE 14 Typical instrumentation view: A, plan; elevations: B, north; C, west [Colour figure can be viewed at wileyonlinelibrary.com]

precast columns (not shown in Figure 14). The data acquisition system sampling rate was 240 Hz. Two High-Definition video camera recorders,<sup>††</sup> 13 GoPros,<sup>‡‡</sup> and 11 closed circuit cameras were deployed to provide overall and close-up video of the specimen. A payload project provided rooftop GPS measurements.<sup>31</sup>

<sup>††</sup>Sony, HDR-CX560.

<sup>‡‡</sup>HD HERO 2.

### 4.4 | Structural response calculations

Key structural responses presented in this paper are calculated using the measured sensor data described in Section 4.3. Due to the unique nature of the IFAS, distinct inter-story drift and acceleration values exist for both the LFRS and GLRS (indicated with the shorthand subscript LS and GS, respectively), and due to the test specimen LFRS plan eccentricity, GLRS responses are reported for the EW and NS direction (with ^ indicating maximum in plan), and total vector sums. Figure 15 provides a schematic of key kinematic responses, shown in their positive sense, and the measurements used to calculate them. Note that redundancy in measurement (multiple string pots, GPS) and calculation (integration of acceleration) allow for independent checks on response.

The calculated kinematic responses for the LFRS include (measured data is indicated in **bold**): (1) wall base in-plane rotation  $\theta_{wall}$  (see Figure 15A) based on the difference of linear pot measurements  $\delta_1, \delta_2$  at each end of the wall base, for all 3 walls ( $\theta_{wall}^N, \theta_{wall}^W, \theta_{wall}^E$ ); (2) LFRS inter-story drift ratio in the EW direction at story  $i$ ,  $\Delta_{LS,i}^{EW}$ , back-calculated from the absolute GLRS displacement in line with the North wall  $u_i^N$  (extrapolated from measured displacements  $u_i^B, u_i^C$  using rigid body floor kinematics, Figure 15C) and the relative displacement between the North wall and the floor slab,  $\delta_{r,i}^N$ :

$$\theta_{wall} = (\delta_1 - \delta_3) / d_{13} \tag{1}$$

$$\Delta_{LS,i}^{EW} = \left( (u_i^N - \delta_{r,i}^N) - (u_{i-1}^N - \delta_{r,i-1}^N) \right) / h_i \tag{2}$$

where  $h_i$  is floor-to-floor height of the  $i^{th}$  story. In the orthogonal direction,  $\Delta_{LS,i}^{NS}$  can be similarly calculated with relative displacement  $\delta_{r,i}^W, \delta_{r,i}^E$  measured between the transverse walls and slab.

The calculated kinematic responses for the GLRS include (1) GLRS inter-story drift ratio at story  $i$ ,  $\Delta_{GS,i}^{(EW \text{ or } NS)}$  (Figure 15B), defined as the relative horizontal displacement of two adjacent floors in a direction divided by the story height. This value is: (a) calculated in each direction (EW or NS) using the diagonal string pots (Figure 15b), where  $L_{jk}$  and  $L_d$  represent the horizontal and diagonal bay dimensions and  $\delta_{d,i}$  represents the measured string pot displacement; (b) checked at the location of maximum twisting-amplified drift in the EW direction along column line C using directly measured absolute GLRS displacements  $u_i^C$ , which coincides with one of the diagonal string pots arrays; (c) checked at the location of North wall using the calculated GLRS displacement  $u_i^N$ :

$$\Delta_{GS,i}^{(EW \text{ or } NS)} = \left( \sqrt{(L_d + \delta_{d,i})^2 - h_i^2} - L_{jk} \right) / h_i \tag{3a}$$

$$\hat{\Delta}_{GS,i}^{EW} = (u_i^C - u_{i-1}^C) / h_i \tag{3b}$$

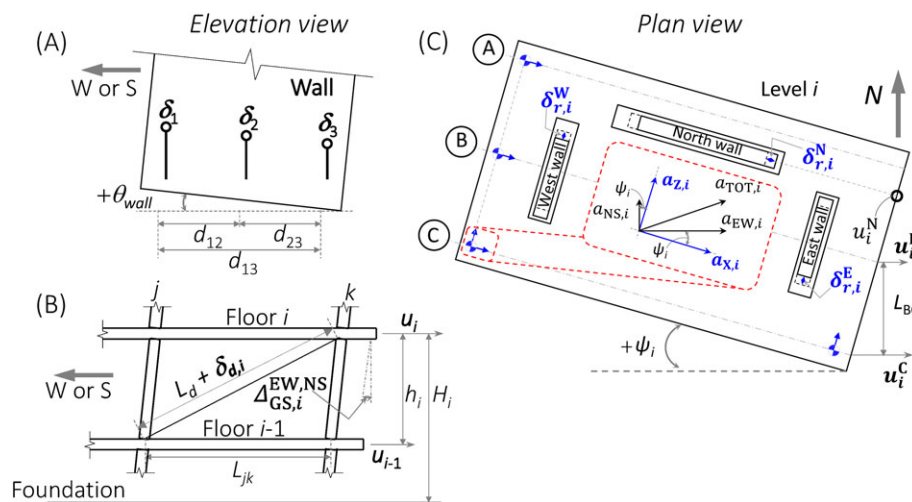


**FIGURE 15** Structure response kinematics: A, wall base rotation; B, GLRS drift ratio; C, slab twist [Colour figure can be viewed at wileyonlinelibrary.com]

$$\Delta_{GS,i}^N = (u_i^N - u_{i-1}^N) / h_i \quad (4)$$

(2) the resultant maximum GLRS inter-story drift ratio (at column C3),  $\hat{\Delta}_{GS,i}^{TOT}$ , calculated as

$$\hat{\Delta}_{GS,i}^{TOT} = \sqrt{\hat{\Delta}_{GS,i}^{EW\ 2} + \hat{\Delta}_{GS,i}^{NS\ 2}} \quad (5)$$

Then, (3) slab twist angle in plan at level  $i$ ,  $\psi_i$  (Figure 15C) calculated as

$$\psi_i = (\mathbf{u}_i^B - \mathbf{u}_i^C) / L_{BC} \quad (6)$$

Finally, (4) floor acceleration corrected for twisting (Figure 15C) at level  $i$  given by

$$a_{EW,i} = \mathbf{a}_{X,i} \cos\phi_i + \mathbf{a}_{Z,i} \sin\phi_i \quad (7a)$$

$$a_{NS,i} = \mathbf{a}_{X,i} \sin\phi_i - \mathbf{a}_{Z,i} \cos\phi_i \quad (7b)$$

$$\hat{a}_{TOT,i} = \sqrt{\hat{a}_{EW,i}^2 + \hat{a}_{NS,i}^2} \quad (7c)$$

where  $\mathbf{a}_{(X\ or\ Z),i}$ ,  $a_{(EW\ or\ NS),i}$ , and  $\hat{a}_{TOT,i}$  are the measured, corrected, and maximum (in plan) total accelerations, respectively. A 33-Hz low-pass filter was applied to the accelerations.

## 5 | SHAKE-TABLE TEST RESULTS

Shake-table test results presented in Sections 5.1 to 5.5 focus on the comparison between the IFAS structure (Phase I) and the comparable conventional structure (Phase II). Comparisons take place at 4 ascending levels of seismic demand: SE DBE, BE SVC, BE DBE, and BE MCE levels, using the tests shaded in gray in Table 9. In the plots, IFAS structure response is shown as black lines; conventional structure response is shown as gray lines. A limited number of Phase III comparisons appear in Section 5.4. Section 5.6 discusses certain experimental results in the context of the anticipated response. All data presented are directly measured or calculated from the actual tests, thus represent half-scale response. The reader is referred to Table 8 for guidance in scaling to a full-scale prototype.

### 5.1 | LFRS response comparison: IFAS vs conventional

A comparison of LFRS response between the IFAS and conventional structures is considered. As PT rocking walls were used, LFRS demands are expressed as wall base in-plane rotation. Figure 16 compares the North wall base rotation time histories. The results indicate significant LFRS demand reduction in the table motion direction for the IFAS structure relative to the conventional structure for the first 3 demand levels. Note that the North wall response reduction was not as significant in the BE MCE (see Figure 16D) as in other hazard levels. This finding is considered in the context of the structure orthogonal response, as discussed next for the transverse walls.

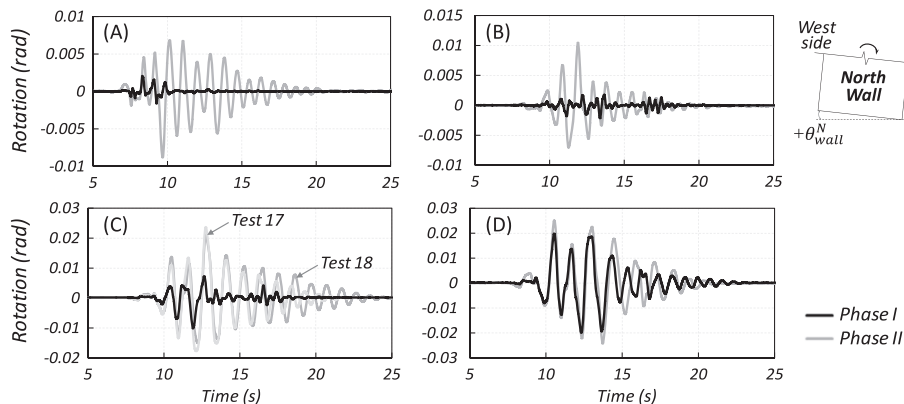


**FIGURE 16** North wall base in plane rotation  $\theta_{wall}^N$ : A, SE DBE; B, BE SVC; C, BE DBE; D, BE MCE

Figure 17 shows the base rotation comparison, this time for the (west) transverse wall. The plots indicate similar transverse wall response for IFAS and conventional structures at lower demand (no or little reduction), but a significant response reduction in the IFAS structure for the two stronger motions (see Figure 17C,D).

The results in Figures 16 and 17 indicate an increasing importance of the torsional response over the longitudinal translational response in the stronger earthquakes, with the torsional response of the conventional structure much greater than the IFAS structure. This aspect is treated further in Section 5.3, which demonstrates that when considering *total* structure response for this asymmetric building, the IFAS is seen to significantly reduce the LFRS demands at *all* earthquake levels.

### 5.2 | GLRS response comparison: IFAS vs conventional

Figure 18 shows the GLRS inter-story drift envelopes,  $\hat{\Delta}_{GS}^{EW}$  and  $\hat{\Delta}_{GS}^{TOT}$ , for different seismic demand levels. As seen, the maximum GLRS drifts, both EW and total, are consistently lower for the IFAS structure than for the conventional structure. This positive result was not necessarily anticipated and is discussed further in Section 5.6. Recall from Table 8 that these results can be used directly for interpretation of a full-scale prototype.

### 5.3 | Building overall response comparison: IFAS vs conventional

Figure 19A-D shows slab twisting angle, ( $\psi$ ) envelopes for Phases I and II. The slab twisting is similar in the smaller earthquakes; however, the IFAS is seen to significantly reduce building torsion in plan for the stronger earthquakes, where a dominant torsional mode was observed (Figure 17).

Figure 19E compares different maximum drift response profiles along the structure height for Phases I and II for the BE MCE. The results illustrate the relationship between LFRS and GLRS inter-story drifts in an IFAS structure. As a

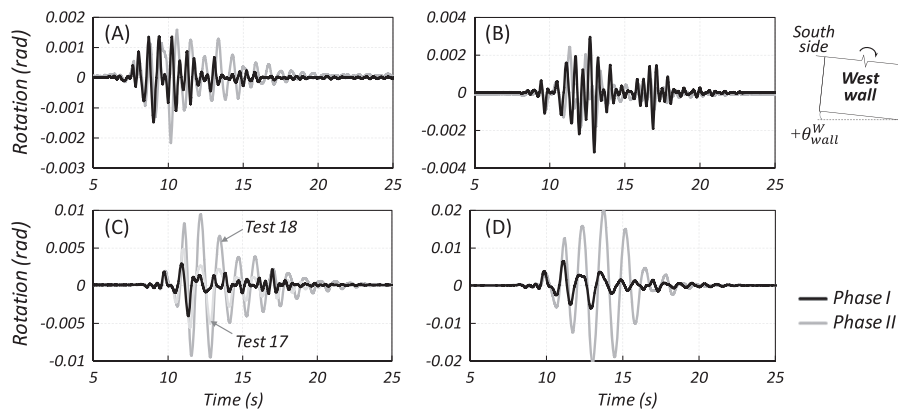


FIGURE 17 West wall base in plane rotation  $\theta_{wall}^W$ : A, SE DBE; B, BE SVC; C, BE DBE; D, BE MCE

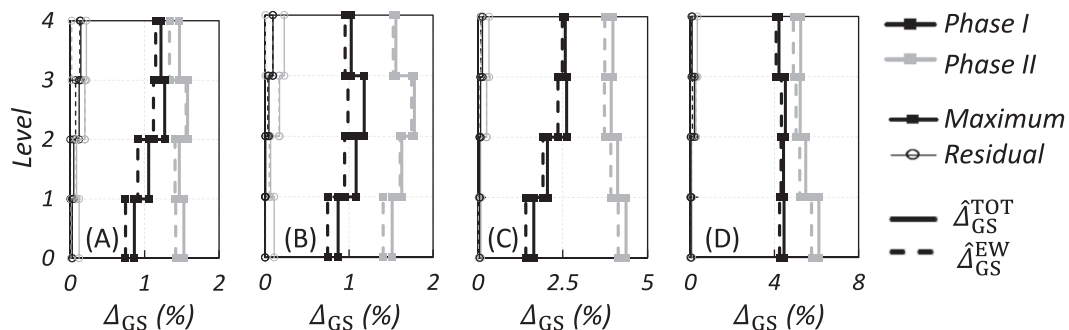


FIGURE 18 Max GLRS inter-story drift ratio  $\hat{\Delta}_{GS}^{EW}$ ,  $\hat{\Delta}_{GS}^{TOT}$ : A, SE DBE; B, BE SVC; C, BE DBE; D, BE MCE

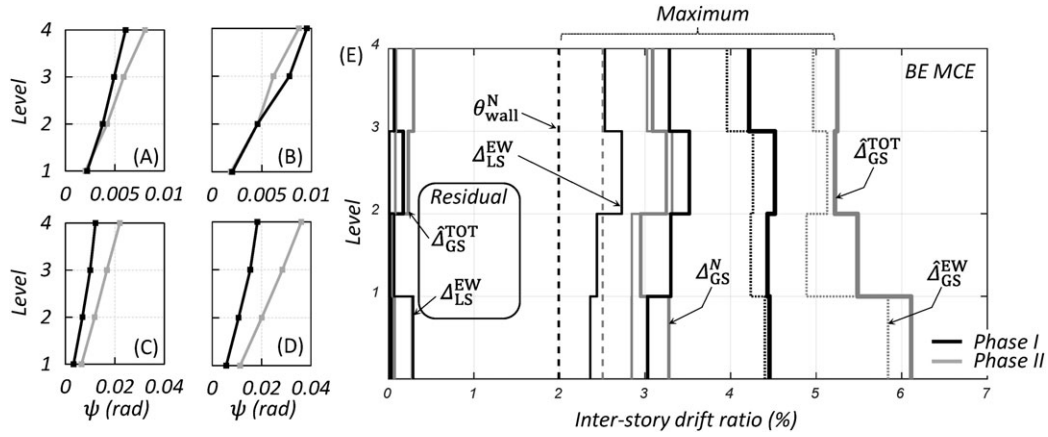


FIGURE 19 Slab twisting  $\psi$  envelope: A, SE DBE; BE: B, SVC; C, DBE; D, MCE; E, BE MCE inter-story drift

reference, the North wall base rotations  $\theta_{wall}^N$  are indicated as vertical dashed trend lines. The first set of solid lines to the right of the trend lines indicate the inter-story drift ratio of the North wall  $\Delta_{LS}^{EW}$ . The larger variation in the LFRS inter-story drift ratio for Phase II may be due to larger higher mode effects for the conventional structure. The adjacent thicker solid lines represent the GLRS drift in the EW direction at the North wall,  $\Delta_{GS}^N$ . Note the significant difference in the LFRS and GLRS drift for the IFAS structure due to the partial uncoupling of these elements. Also note that the “conventional” structure specimen approaches but does not exactly realize a rigid diaphragm condition. Given the structural eccentricity in plan, the maximum EW drift  $\Delta_{GS}^{EW}$  occurs at the south perimeter and is significantly larger than at the wall, as shown in the next (dotted) lines. Finally, the resultant drift  $\hat{\Delta}_{GS}^{TOT}$  is somewhat larger, in particular for the conventional structure, which exhibited larger in-plan twist. As seen, even with the floor relative displacements in the IFAS, the total drifts are significantly larger for the conventional structure. Residual drifts are also shown and seen to be small, but slightly larger in the “conventional” structure.

To estimate overall demands in the BE MCE for the coupled translational/torsional system, consider the response of all three walls, shown in Figure 20A as cumulative base rotation, for each individual wall and for the total of 3 walls. This approximate index of overall demands indicates a significant response reduction for the IFAS structure, clarifying the conflicting results of Figures 16D and 17D. Note also the asymmetry of response in the conventional structure (Phase II East vs West wall) in comparison to the IFAS structure.

Figure 20B,C shows time histories of the fourth story GLRS inter-story drift ratio at column line C,  $\hat{\Delta}_{GS,4}^{EW}$ , for the lower demand earthquakes, indicating that comparing maxima, which are similar, does not fully reveal the response reduction in terms of cumulative demands, which are seen to be significantly lower in the IFAS structure.

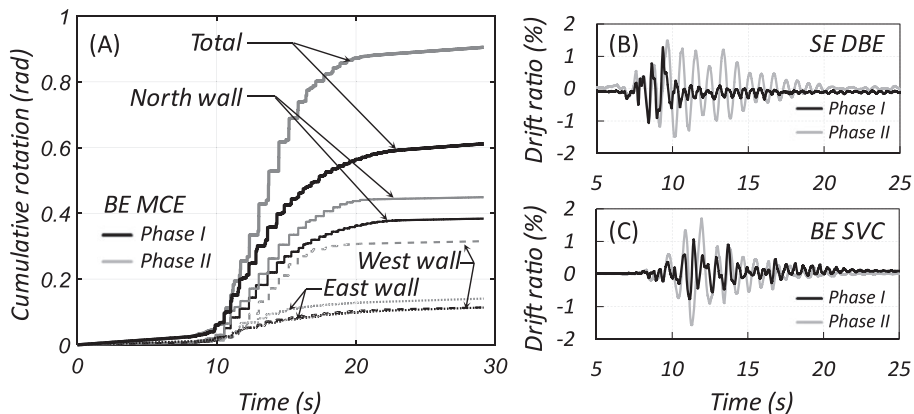


FIGURE 20 A, BE MCE cumulative base rotation; GLRS EW fourth story drift ratio,  $\hat{\Delta}_{GS,4}^{EW}$ ; B, SE DBE; C, BE SVC

### 5.4 | Floor acceleration response comparison: IFAS vs conventional

Figure 21 shows the maximum EW direction and total floor accelerations  $\hat{a}_{EW}$ ,  $\hat{a}_{TOT}$  for different earthquake demand levels. The acceleration comparison also includes the Phase III structure (Figure 21C,D) for the BE DBE and BE MCE motions. The results indicate similar maximum floor acceleration in Phases I and II, and higher in Phase III. Recall from Table 8 that these results can be used directly for interpretation of a full-scale prototype.

### 5.5 | Floor anchorage comparison: IFAS vs conventional

Figure 22 shows time histories of fourth floor relative displacement at different earthquake levels for the North wall (EW direction)  $\delta_{r,4}^N$ , shown here at the center-of-slab elevation. These displacements are approximately equal to the FD and PSA deformations; however, as the former was installed underneath the slab and the latter was placed at the top of the slab, a different correction is needed for each due to the PT wall rotation. The bumper initial gap  $g_0$  (Figure 2B) is indicated with horizontal dashed lines in Figure 22.

Consistent with the IFAS design intent (Figure 4B), the bumper was not engaged in smaller earthquakes, only infrequently engaged under modest deformation in the DBE; but “bottoms-out” several times during the MCE event, thereby arresting the floor relative displacement. None of the relative displacements are seen to exceed the target displacement design limit. Recall that these displacements (and those shown in Figure 23) are at half-scale and need to be doubled for interpretation of a full-scale prototype (Table 8).

Examining the Phase II response, eg, Figure 22, SE DBE, it is important to note that the PSA diaphragm connection (Figure 10B) did deform, as expected, and thus was not as “rigid” an anchorage as might be anticipated for dowel bars in a cast-in-place floor. Deformations did remain below the yield displacement (Figure 12B), and thus the PSA was assumed to remain at elastic force levels. The roller bearing introduced in Test 18 is seen to reduce the relative displacement as desired (compare Tests 17, 18 in Figure 22C). Note that the floor did not return exactly to zero position after each test, as indicated by the initial offsets.

Figure 23A shows the residual relative displacement of the roof level after each test, showing measurable but not excessive residual displacement. Figure 23B,C shows selected force-deformation response of the force-limiting

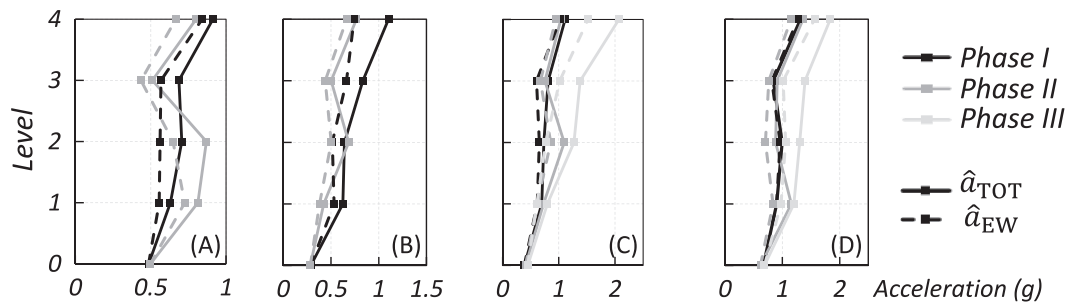
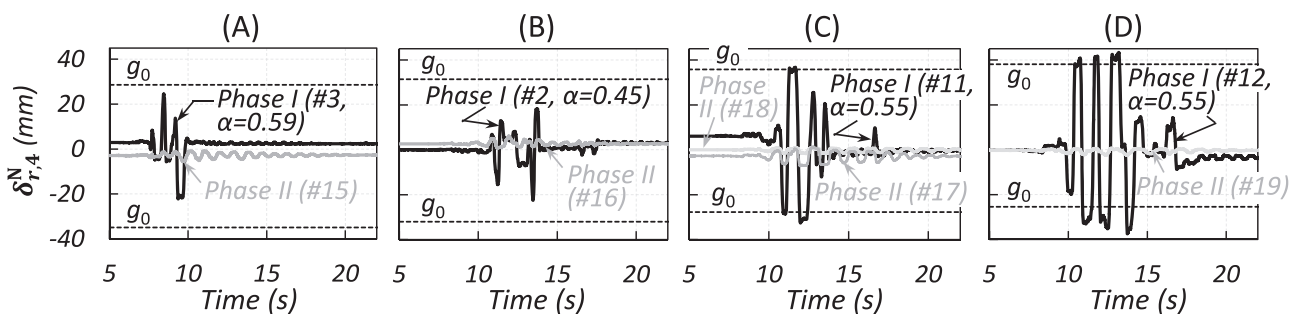
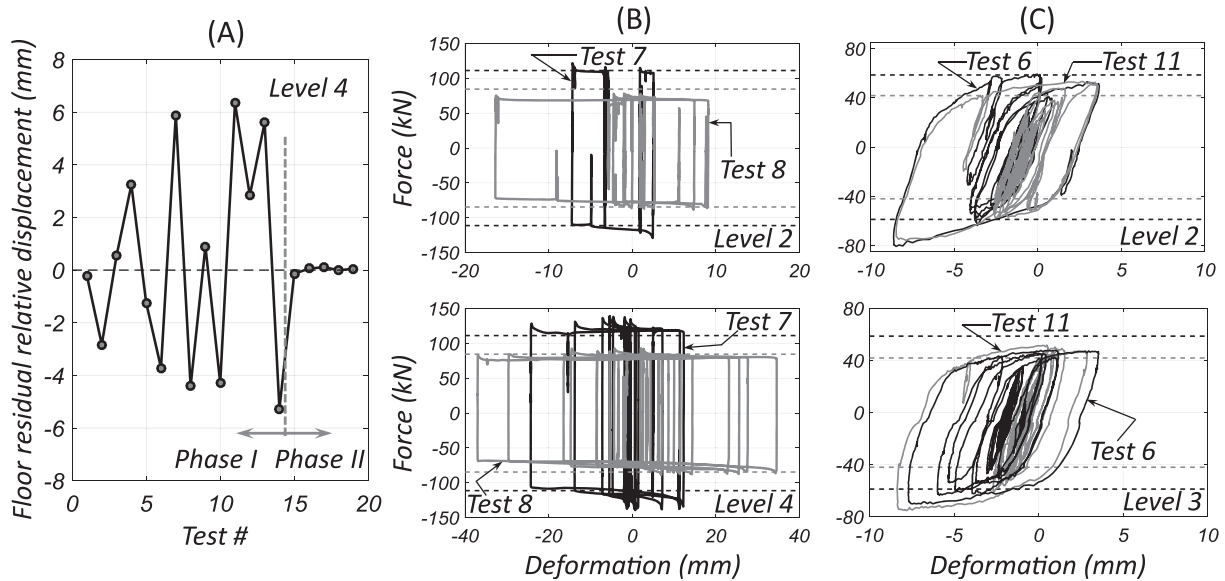


FIGURE 21 GLRS acceleration envelope: A, SE DBE; B, BE SVC; C, BE DBE; D, BE MCE



Note: The “#” in this figure represents “Test numbering”.

FIGURE 22 Roof relative displacement in EW direction: A, SE DBE; B, BE SVC; C, BE DBE; D, BE MCE



**FIGURE 23** A, Floor residual relative displacement; force-deformation response: B, FD; C, BRB

components for different Phase I tests: (B) the FD on the second and fourth levels; (C) the West transverse wall BRB, in this case at the second and third levels. Refer to Table 8 for scaling these forces for interpretation of a full-scale prototype.

The FD provides stable and efficient hysteretic response (Figure 23B), exhibiting excellent energy dissipation characteristics. The tests compared in Figure 23B are BE DBE tests with different IFAS design strengths: Test 7 (intermediate,  $\alpha = 0.61$ ); Test 8 (aggressive,  $\alpha = 0.41$ ), as indicated by horizontal trend lines (black and dark gray respectively). As expected, a larger floor relative displacement is seen for a lower IFAS strength. The BRBs also exhibited excellent energy dissipation characteristics (Figure 23C), and in contrast to the FD, work harden under increasing cyclic deformation (Test 11 vs 6). The response of the force-limiting components on other floors also shows stable and efficient (full loops) hysteretic response, as well as a strength close to the design strength. Further information on the force-limiting components appear in Tsampras et al.<sup>4,27,28</sup>

## 5.6 | Further discussion of selected results

Several behaviors of the shake-table test specimen are still under investigation using 3-dimensional models being calibrated to these results, including: the underlying reason for the transformation to a torsion-dominated coupled mode; the potential differences in behavior presented by the use of the PSA and roller bearings in Phase II, rather than a conventional cast-in-place dowel anchorage; and, the contribution of the lower (due to repeatability measures) yet nonetheless extant degradation in the test structure. Further, 2 unanticipated results in the testing, also under analytical investigation for future treatment, warrant further comment here:

- (1) **Lower GLRS drift ratio for the IFAS structure:** This positive result was not always anticipated in the analytical research used to develop the IFAS, where limiting amplified GLRS drift ratio at very low  $\alpha$  values was a major design constraint.<sup>1</sup> However, an intermediate  $\alpha$  range was observed where GLRS drift ratio is seen to lessen relative to stronger designs (refer to slight “valley” in MCE GLRS drift response in Figure 4A). This “valley” was not significant for the RC wall evaluation structure used to develop the design space. However, subsequent analyses<sup>19</sup> have indicated that this “valley” can become pronounced for rocking walls, particularly for low LFRS overstrength and low-rise structures, which all fit the description of the shake-table test specimen. Further, the shake-table test specimen had a slightly stiffer and stronger GLRS in relation to the evaluation structure (refer to Figure 3), also shown to have an effect. Cumulative damage in the test specimen might also have contributed.
- (2) **Similar floor accelerations in Phases I and II:** The similar floor accelerations were not anticipated in the analytical research developing the IFAS, where significant floor acceleration reduction was observed.<sup>1</sup> The reason for this outcome may be due to two factors: (1) the low overstrength of the PT rocking wall (refer to Phase I and II values in Table 6); and, (2) the damage incurred in the structure between Phases I and II. The first conclusion is supported

by the significantly higher accelerations observed in Phase III where a larger wall strength existed (Figure 11B); initial analytical examinations<sup>19</sup> supported the validity of both these conclusions. The low-rise nature of the structure also tends to lower the acceleration reduction afforded by the IFAS,<sup>19</sup> but not to the extent observed in the testing. It should also be noted that for the lower demand Phase II tests (Figure 21A,B), the deformable connections were left in place (refer to Tests 15-17, Table 9) and thus may have provided some unanticipated supplemental energy dissipation. However, these elements were not present for the stronger Phase II tests (Figure 21C,D). Flexibility in the conventional anchorage may have also played a role. The impact of LFRS strength and stiffness, structural damage, supplemental damping, and connection flexibility on floor accelerations in IFAS structures are all being examined using models calibrated to this test.

## 6 | CONCLUSIONS

An innovative floor connecting system, the Inertial Force-Limiting Anchorage System or IFAS, has been developed and evaluated in shake-table testing. The experimental evaluation involved a half-scale 4-story concrete structure that permitted a comparison of the IFAS performance to a conventional structure. The following conclusions are drawn from this test:

- 1 The IFAS was shown to significantly reduce the maximum and cumulative LFRS lateral drift ratios (used in the testing as an equivalent measure of structural damage), thereby indicating the potential to reduce structural damage in earthquakes.
- 2 The IFAS structure exhibited reduced floor accelerations relative to the structure with a stiffer and stronger LFRS, implying the ability to reduce non-structural damage in such structures. The IFAS structure did not demonstrate a significant reduction in floor acceleration with respect to a structure of comparable nominal stiffness and strength. This unanticipated result is attributed to low LFRS overstrength, and damage accrued in the test structure during testing. This result requires further examination through analytical simulation.
- 3 The Gravity Load-Resisting System (GLRS) drift ratios were not amplified in the IFAS structure; in fact, the IFAS structure had lower GLRS drift ratios than the comparable conventional structure. This positive result, not always anticipated in earlier analytical research, is attributed to the nature of rocking wall structure response, a combination of low LFRS overstrength and low-rise structures, and the stiffness and strength of the GLRS, and requires further examination through analytical simulation.
- 4 The force-limiting components within the IFAS, both FDs and BRBs, provided well-controlled strength, good energy dissipation, and sufficient deformation capacity to serve as effective devices for the IFAS. Some remaining issues for using a full-scale FD in an actual implementation are reported in Tsampras et al.<sup>27</sup>
- 5 The IFAS assemblage, FD or BRBs, RBs and bumpers, was able to perform as intended as a system, including the FD and BRB providing controllable force limiting and energy dissipation under the complex kinematics of an eccentric rocking wall structure; the RBs providing LFRS stabilization and restoring forces to minimize floor residual displacements; and the bumper limiting the relative displacement of the floor.
- 6 The feasible design space identified from analytical parameter studies successfully produced an effective IFAS design and can be used as the basis for developing a design procedure for the IFAS and IFAS structure.

The results of the test program indicate that the IFAS has the potential to reduce building response during earthquakes. Some unresolved issues remain based on the observed test results and are under investigation using evaluation structure models<sup>19</sup> calibrated to the shake-table test results:

- 1 Determination of the factors that affect: (1) floor acceleration reduction efficiency in IFAS structures; and, (2) GLRS inter-story drift ratio amplification or reduction in IFAS structures.
- 2 Examination of the increased role of the coupled translational-torsional mode in stronger earthquakes.
- 3 Evaluation of the impact of damage and the simulated traditional anchorage on the Phase II response.

Using the shake-table test results and the subsequent analytical work, design procedures can be developed for the use of the IFAS in low-damage building structures.



## ACKNOWLEDGEMENTS

This research was supported by the National Science Foundation (NSF) under Grant CMMI-1135033, Network for Earthquake Engineering Simulation Research (NEESR). Additional support was provided by the Prestressed/Precast Concrete Institute (PCI), the Charles Pankow Foundation, PCI West, Clark Pacific, and the “Fund of Social Development” grant (№KФ-14/03) at the Nazarbayev University. Material and device donations provided by industry partners Star Seismic, MMFX, Davis Wire, DYMAT, JVI Inc., Pleiger Inc., Wire Reinforcement Institute, FYFE, BASF Inc., Gerdau Inc., HRC Inc., Core Slab, Dura Fiber, and Triton Structural Concrete. Engineering and construction services provided by industry partners Midstate Precast, T.B. Penick & Sons, Brewer Crane & Rigging, Atlas Construction Supply, Western Concrete pumping, and Steel City Scaffold. The authors are grateful for this support. Any opinions, findings, conclusions, or recommendations expressed in this material are those of the author(s) and do not necessarily reflect the views of the NSF or co-funders.

## ORCID

Zhi Zhang  <http://orcid.org/0000-0002-8205-5384>

Georgios Tsampras  <http://orcid.org/0000-0001-8255-3415>

## REFERENCES

1. Zhang D, Fleischman R, Restrepo J, et al. (2014). Development of a floor inertia force limiting anchorage system under earthquake loading. 10th NCEE, Anchorage, Alaska, 2014.
2. Fleischman R, Restrepo J, Nema A, et al. (2015) Inertial force-limiting anchorage system for seismic resistant building structures. ASCE Structures Congress 2015.
3. ASCE/SEI 7. *Minimum Design Loads for Buildings and Other Structures*. ASCE; 2010.
4. Tsampras G, Sause R, Zhang D, et al. Development of deformable connection for earthquake-resistant buildings to reduce floor accelerations and force responses. *Earthquake Eng Struct Dynam*. 2016;45(9):1473-1494.
5. Skinner RI, Kelly JM, Heine AJ. Hysteretic dampers for earthquake-resistant structures. *Earthquake Eng Struct Dynam*. 1975;3(3):287-296.
6. Key DE. The seismic performance of energy absorbing dampers in building structures. *Bull New Zealand Soc Earthquake Eng*. 1984;17(1):38-46.
7. Luco JE, De Barros FCP. Control of the seismic response of a composite tall building modelled by two interconnected shear beams. *Earthquake Eng Struct Dynam*. 1998;27(3):205-223.
8. Mar D, Tipping S. *Smart Frame Story Isolation System: A New High-Performance Seismic Technology*. Berkeley, California: Tipping Mar + Associates; 2000.
9. Crane ST. Influence of energy dissipation connections between floors and the lateral force resisting system. Master Thesis, University of California, San Diego, San Diego, California; 2004.
10. FEMA E-74. Reducing the risks of nonstructural earthquake damage—a practical guide 2012.
11. Rodriguez ME, Restrepo JI, Carr AJ. Earthquake-induced floor horizontal accelerations in buildings. *Earthquake Eng Struct Dynam*. 2002;31(3):693-718.
12. NEESR meeting. Minutes, NEESR Project Meeting #3, Rutherford & Chekene Offices, San Francisco; 2012.
13. Pall AS. Limited slip bolted joints—a device to control seismic response of large panel structures. Ph.D. Dissertation, Concordia University, Montreal, Quebec, Canada; 1979.
14. Chi B, Uang CM. Dynamic testing of full-scale slotted bolted connections. Report No. TR-99/05. Department of Structural Engineering, University of California, San Diego; 2000.
15. Watanabe A, Hitomi Y, Saeki E, Wada A, Fujimoto M. Properties of brace encased in buckling-restraining concrete and steel tube. Proceedings of 9th WCEE, August 2–9, Tokyo-Kyoto, Japan; 1988.
16. Fahnestock LA, Sause R, Ricles JM. Seismic response and performance of buckling-restrained braced frames. *J Struct Eng, ASCE*. 2007;133(9):1195-1204.
17. Huang YN, Whittaker AS, Luco N. Seismic performance assessment of base-isolated safety-related nuclear structures. *Earthquake Eng Struct Dynam*. 2010;39(13):1421-1442.
18. Luo J, Wierschem N, Fahnestock L, et al. Realization of a strongly nonlinear vibration-mitigation device using elastomeric bumpers. *J Eng Mech*. 2014;140(5). [https://doi.org/10.1061/\(ASCE\)EM.1943-7889.0000692](https://doi.org/10.1061/(ASCE)EM.1943-7889.0000692), 04014009

19. Zhang Z.. Analytical investigation of inertial force-limiting floor anchorage system for seismic resistant building structures, Ph.D. Dissertation, University of Arizona; 2017.
20. Restrepo JI, Conte JP, Luco JE, Seible F, Van Den Einde L. The NEES@UCSD large high performance outdoor shake table. Geo-Frontiers Congress 2005, Austin, TX, Jan. 24–26, 2005. [https://doi.org/10.1061/40779\(158\)1](https://doi.org/10.1061/40779(158)1)
21. Holden TJ. A comparison of the seismic performance of precast wall construction: emulation and hybrid approaches. Master Thesis, University of Canterbury, Christchurch, New Zealand; 2001.
22. Kurama Y, Pessiki S, Sause R, Lu LW. Seismic behavior and design of unbonded post-tensioned precast concrete walls. *PCI J.* 1999;44(3):72-89.
23. Ghosh SK, Hawkins NM. Codification of PRESSS structural systems. *PCI J.* 2003;48(4):140-143.
24. Restrepo JI, Rahman A. Seismic Performance of Self-Centering Structural Walls Incorporating Energy Dissipators. *J Struct Eng ASCE.* 2007;133(11):1560-1570.
25. Belleri A, Schoettler MJ, Restrepo J, Fleischman RB. Dynamic behavior of rocking and hybrid cantilever walls in a precast concrete building. *ACI Struct J.* 2014;111(3):661-672.
26. Toranzo-Dianderas L. The use of rocking walls in confined masonry structures: a performance-based approach. Ph.D. Dissertation, the University of Canterbury; 2002.
27. Tsampras G, Sause R, Fleischman RB, Restrepo JI. Experimental study of deformable connection consisting of friction device and rubber bearings to connect floor system to lateral force resisting system. *Earthquake Eng Struct Dynamics.* 2016;47(4):1032-1053.
28. Tsampras G, Sause R, Fleischman RB, Restrepo JI. Experimental study of deformable connection consisting of buckling restrained brace and rubber bearings to connect floor system to lateral force resisting system. *Earthquake Eng Struct Dynam.* 2016;46(8):1287-1305.
29. Guerrini G, Restrepo J, Massari M, Vervelidis A. Seismic behavior of posttensioned self-centering precast concrete dual-shell steel columns. *J Struct Eng ASCE.* 2015;141(4):04014115.
30. JVI. PSA slotted inserts for precast concrete panel connections. 7131 N Ridgeway Avenue, Lincolnwood, IL 60712, USA; 1993. <http://www.jvi-inc.com>
31. Saunders JK, Goldberg DE, Haase JS, et al. Seismogeodesy using GPS & low-cost MEMS accelerometers: perspectives for earthquake early warning & rapid response. *Bull Seismol Soc Am.* 2016;106(6):2469-2489.

**How to cite this article:** Zhang Z, Fleischman RB, Restrepo JI, et al. Shake-table test performance of an inertial force-limiting floor anchorage system. *Earthquake Engng Struct Dyn.* 2018;47:1987–2011. <https://doi.org/10.1002/eqe.3047>